

## Response to the editor's comments

Overall the manuscript is much improved. I have made some additional suggestions in the attached pdf, where the phrasing and grammar still requires some changes to ensure that your statements are clear. Please check these carefully, including the figure captions.

There is still a need for you to add some more detail to your discussion of the climatic implications of your findings, in the final Discussion paragraph. At present this paragraph is reliant on the paper by Ning et al. 2019 but it is presented very factually, rather than highlighting debate and uncertainties (and where your data sets could contribute to addressing these).

You should also refer carefully to the Climate of the Past data policy ([climate-of-the-past.net/about/data\\_policy.html](http://climate-of-the-past.net/about/data_policy.html)). Your data needs to be available in a publically accessible database, not just 'available on request'. Many of the databases allow you to embargo release of the datasets while publications are under review.

**Response:** *We have revised the manuscript according your comments. Firstly, we modified the manuscript following the suggestions in the PDF, and we again checked the phrasing and grammar. Secondly, we reorganized the discussion of section 4.2 to make the statement more clear. However, the isoGDGTs in Lake Chenghai sediments are dominated by GDGT-0 and Cren, and a significant negative correlation is found in this study. Therefore, we suggest that the ratio of GDGT-0/Cren may have originated from a similar mechanism to %cren values, and hence we do not discuss the proxy further. Thirdly, we have expanded the dynamics of temperature evolution during the early to middle Holocene. The influences of solar insolation and the status of Northern Hemisphere ice-sheets are presented in more detail. Lastly, we modified the figures and have made the data available in the supplementary information.*

1 **Archaeal lipid-inferred paleohydrology and paleotemperature of**  
2 **Lake Chenghai during the Pleistocene-Holocene transition**

3 Weiwei Sun <sup>a</sup>, Enlou Zhang <sup>a,b,\*</sup>, Jie Chang <sup>a</sup>, James Shulmeister <sup>c,d</sup>, Michael I. Bird <sup>e</sup>,  
4 <sup>f</sup>, Cheng Zhao <sup>a,b</sup>, Qingfeng Jiang <sup>g</sup>, Ji Shen <sup>a</sup>

5 <sup>a</sup> State Key Laboratory of Lake Science and Environment, Nanjing Institute of  
6 Geography and Limnology, Chinese Academy of Sciences, Nanjing 210008, China

7 <sup>b</sup> Center for Excellence in Quaternary Science and Global Change, Chinese Academy  
8 of Science, Xian 710061, China

9 <sup>c</sup> School of Earth and Environmental Sciences, The University of Queensland, St  
10 Lucia, Brisbane, Qld, 4072, Australia

11 <sup>d</sup> School of Earth and Environment, University of Canterbury, Private Bag 4800,  
12 Christchurch, New Zealand

13 <sup>e</sup> ARC Centre of Excellence for Australian Biodiversity and Heritage, James Cook  
14 University, PO Box 6811, Cairns, Queensland, 4870, Australia

15 <sup>f</sup> College of Science and Engineering, James Cook University, PO Box 6811, Cairns,  
16 Queensland, 4870, Australia

17 <sup>g</sup> School of Geography Sciences, Nantong University, Nantong, 226007, China

18 | \* Corresponding authors. [elzhang@niglas.ac.cn](mailto:elzhang@niglas.ac.cn). State Key Laboratory of Lake  
19 Science and Environment, Nanjing Institute of Geography and Limnology, Chinese  
20 Academy of Sciences, Nanjing 210008, China

21

22

23

24

25 **ABSTRACT**

26 Over the past decades, paleoenvironmental studies in the Indian Summer  
27 Monsoon (ISM) region have mainly focused on precipitation change, with few  
28 published terrestrial temperature records from the region. We analyzed the distribution  
29 of isoprenoid glycerol dialkyl glycerol tetraethers (isoGDGTs) in the sediments of  
30 Lake Chenghai in southwest China across the Pleistocene–Holocene transition, to  
31 extract both regional hydrological and temperature signals for this important transition  
32 period. Lake-level was reconstructed from the relative abundance of crenarchaeol in  
33 isoGDGTs (%cren) and the crenarchaeol'/crenarchaeol ratio. The %cren-inferred  
34 lake-level identified a single lowstand (15.4-14.4 cal ka BP), while the  
35 crenarchaeol'/crenarchaeol ratio suggests relatively lower lake-level between  
36 15.4-14.4 cal ka BP and 12.5-11.7 cal ka BP, corresponding to periods of weakened  
37 ISM during the Heinrich 1 and Younger Dryas cold event. A filtered TetraEther index  
38 consisting of 86 carbon atoms (TEX<sub>86</sub> index) revealed that lake surface temperature  
39 was similar to present-day values during the last deglacial period, and suggests a  
40 substantial warming of ~4 °C from the early Holocene to the mid-Holocene. Our  
41 paleotemperature record is generally consistent with other records in southwest China,  
42 suggesting that the distribution of isoGDGTs in Lake Chenghai sediments has  
43 potential for quantitative paleotemperature reconstruction.

44

45 **Keywords:** Quantitative temperature reconstruction; Lake-level; TEX<sub>86</sub>; Isoprenoid  
46 GDGTs; Lacustrine sediment

47

48

49

50

51

## 52 1. Introduction

53 Precipitation variation in the Indian summer monsoon (ISM) region has a ~~great~~  
54 ~~threat to~~ strong influence over ecosystem function, water availability and economic  
55 security across the region (Sinha et al., 2011; Sinha et al., 2015; Ljungqvist et al.,  
56 2016). As a result, This has stimulated growing scientific interest has been stimulated  
57 in understanding the underlying forcing mechanisms behind climate variability in the  
58 ISM region on a range of time-scales, in order to better predict future monsoonal  
59 variations. Over the past two decades, climate evolution in the ISM region since the  
60 Last Glacial Maximum has been reconstructed from various paleoclimatic archives,  
61 including speleothems, and marine/lacustrine sediments (Dykoski et al., 2005; Rashid  
62 et al., 2007; Govil and Divakar Naidu, 2011; Saraswat et al., 2013; Contreras-Rosales  
63 et al., 2014; Wang et al., 2014b; Dutt et al., 2015; Wu et al., 2015; Kathayat et al.,  
64 2016; Zhang et al., 2017a, 2017b; Li et al., 2018; Zhang et al., 2018; Sun et al., 2019;  
65 Zhang et al., 2019). These studies provide evidence of changes in ISM precipitation  
66 on orbital- and millennial time-scales, with a weakened ISM occurring during cold  
67 events, and strengthened ISM occurring during warm intervals.

68 In addition to precipitation, temperature is an important climatic factor, due to its  
69 significant effects on evaporation and regional hydrological cycle. There remains a  
70 lack of quantitative reconstructions of terrestrial temperature from the ISM region  
71 (Shen et al., 2006; Zhang et al., 2017a; Wu et al., 2018; Feng et al., 2019; Ning et al.,  
72 2019; Tian et al., 2019; Zhang et al., 2019). During the last deglaciation-Holocene  
73 transition, the climate of high latitudes in the Northern Hemisphere is punctuated by  
74 three abrupt, millennial-scale events: the Heinrich 1 (H1) cold event, the  
75 Bølling/Allerød (BA) warm period and the Younger Dryas (YD) cooling (Alley and  
76 Clark, 1999). These intervals are attributed to a variety of mechanisms including  
77 changes to orbitally-controlled insolation, ice sheet extent, oceanic circulation and  
78 atmospheric greenhouse concentrations (Alley and Clark, 1999). The recent  
79 quantitative summer temperature proxy based on pollen and chironomids from  
80 southwest China has been developed to address the response of long-term temperature

81 to the high latitude climate changes (Zhang et al., 2017 and 2019; Wu et al., 2018).  
82 However, the magnitude of these temperature variations is not consistent, and further  
83 studies are required.

84 Glycerol dialkyl glycerol tetraethers (GDGTs) have been widely used for the  
85 quantitative reconstruction of terrestrial paleotemperature during the Quaternary due  
86 to the fact that they are ubiquitous in soils and lacustrine sediments (Blaga et al., 2013;  
87 Wang et al., 2017b; Zheng et al., 2018; Ning et al., 2019; Tian et al., 2019).  
88 Isoprenoid GDGTs (isoGDGTs), comprising acyclic or ring-containing isoprenoidal  
89 biphytanyl carbon chains, are a suit of membrane lipids produced by some species  
90 of archaea, such as Euryarchaeota, ~~Crenarchaeota~~ and Thaumarchaeota (Schouten et  
91 al., 2013). IsoGDGTs containing 0 to 3 cyclopentane moieties (isoGDGTs 0–3, Fig.  
92 S1) are common isoGDGTs with a large range of biological sources (Schouten et al.,  
93 2013). For example, Thaumarchaeota were the dominant biological source of  
94 GDGT-0 in Lake Lucerne from Switzerland (Blaga et al., 2011); while GDGT-0 in  
95 Lake Challa surface sediments might predominantly derive from archaea residing in  
96 the deeper, anoxic water column, such as group 1.2 and marine benthic group C group  
97 of the Crenarchaeota, and the Halobacteriales of the Euryarchaeota (Sinninghe Damsté  
98 et al., 2009; ~~;) and m~~ Methanogenic and methanotrophic archaea can also be two  
99 important sources of GDGT-0 within the water column and sediment (Blaga et al.,  
100 2009; Powers et al., 2010). In contrast, crenarchaeol and its regioisomer, crenarchaeol'  
101 (Fig. S1), are considered to be produced specifically by mesophilic Thaumarchaeota  
102 in aquatic environments (Schouten et al., 2002; Blaga et al., 2009; Kim et al., 2010;  
103 Powers et al., 2010; Schouten et al., 2013). On this basis, the ratio of  
104 GDGT-0/crenarchaeol has been proposed to evaluate the influence of Thaumarchaeota  
105 on the distribution of isoGDGTs in lacustrine sediments, and the ratio typically varies  
106 between 0.2 and 2 in Thaumarchaeota (Schouten et al., 2002; Blaga et al., 2009).

107 Thaumarchaeota have a physiological mechanism to increase the weighted  
108 average number of cyclopentane rings in their membrane lipids with growth  
109 temperature (Schouten et al., 2002). Thus the TetraEther indeX consisting of 86

110 carbon atoms (TEX<sub>86</sub> index), which represents the relative number of cyclopentane  
111 moieties in isoGDGT molecules derived from aquatic Thaumarchaeota, has great  
112 potential for use as a paleotemperature proxy in the marine environment and large  
113 lakes (Tierney et al., 2008; Berke et al., 2012; Blaga et al., 2013; Wang et al., 2015).  
114 However, the index may not be a reliable proxy for past temperature in small lakes  
115 due to substantial amounts of soil and/or methanogenic archaea isoGDGTs identified  
116 in the same lacustrine sediment and also due to variability in the depth of isoGDGT  
117 production in aquatic ecosystems (Blaga et al., 2009; Powers et al., 2010; Sinninghe  
118 Damsté et al., 2012a).

119 It has also been shown that crenarchaeol' is only present in low abundance in  
120 most Thaumarchaeota except for the group I.1b Thaumarchaeota, where it is one of  
121 the major isoGDGTs (Kim et al., 2012; Sinninghe Damsté et al., 2012b). The  
122 crenarchaeol'/crenarchaeol ratios for enrichment cultures of group I.1a aquatic  
123 Thaumarchaeota are typically 0.01-0.04, however, for group I.1b Thaumarchaeota  
124 enriched from soils the crenarchaeol'/crenarchaeol ratios are around 0.21 and  
125 substantially higher (Pitcher et al., 2011; Sinninghe Damsté et al., 2012a). In addition,  
126 a likely Group I.1b Thaumarchaeota population inhabiting the subsurface water  
127 column near the anoxic-suboxic boundary was found in Lake Malawi, but the total  
128 production of isoGDGTs by this group appears to be much lower than the  
129 surface-dwelling Thaumarchaeota (Meegan Kumar et al., 2019).

130 In addition, aquatic Thaumarchaeota are nitrifiers, that prefer to live above the  
131 oxycline of relatively deep lakes, as has been observed by a range of lipid biomarker  
132 and DNA based investigations of vertical changes in archaea communities in lake  
133 water columns (Sinninghe Damsté et al., 2009; Blaga et al., 2011; Schouten et al.,  
134 2012; Buckles et al., 2013; Meegan Kumar et al., 2019). Some Thaumarchaeota are  
135 thought to be suppressed by a high light level, which consequently might also inhibit  
136 their ability to thrive near the surface of lakes (Schouten et al., 2013). Further,  
137 Thaumarchaeota are chemoautotrophic and thrive predominantly near the oxycline in  
138 stratified lakes, mainly due to the release of ammonia derived from descending

139 particulate organic matter that is recycled primarily by photoautotrophs or  
140 heterotrophs in the photic zone (Tierney et al., 2010). Consequently, the proportion of  
141 crenarchaeol in isoGDGTs (%cren%) has been suggested as lake-level proxy (Wang  
142 et al., 2014a; Wang et al., 2017a; Wang et al., 2019). However, it has also been  
143 suggested that mixing of the water column will be much more frequent at lowstand  
144 conditions, and therefore periodically or permanently oxic, high nutrient availability  
145 water and enhanced nitrogen cycling would be likely to result in a relatively higher  
146 production of crenarchaeol (Filippi and Talbot, 2005; Sinninghe Damsté et al., 2012).

147 In this study, we present an isoGDGT record spanning the last  
148 deglacial-Holocene transition from Lake Chenghai in the southwest China. Our stable  
149 oxygen isotope ( $\delta^{18}\text{O}$ ) record of authigenic carbonates from Lake Chenghai  
150 previously revealed that drought events occurred from 15.6 to 14.4 cal ka BP and 12.5  
151 to 11.7 cal ka BP corresponding to the H-1 and YD event (Sun et al., 2019). The  
152 present study aims were to (1) identify sources of isoGDGTs in Lake Chenghai  
153 sediments and their linkage, if any, with lake-level variation; (2) test the reliability of  
154 isoGDGT-based proxies as temperature indicators, by comparing our results with  
155 other paleoenvironmental records from adjacent areas, and explore the possible  
156 mechanisms driving temperature variations during the last deglaciation-Holocene  
157 transition in southwestern China.

158

## 159 **2. Materials and methods**

### 160 *2.1. Regional setting*

161 Lake Chenghai (26°27'-26°38'N, 100°38'-100°41'E, Fig. 1A) is a tectonic lake  
162 located in the northwestern part of Yunnan Province (Wang and Dou, 1998). The  
163 current water surface elevation is ~1500 m above sea level (a.s.l.), and the maximum  
164 water depth is ~35 m. The lake is hydrologically closed at present, with a surface area  
165 of ~77 km<sup>2</sup> and a catchment of ~318 km<sup>2</sup> (Wu et al., 2004). However, Lake Chenghai  
166 was linked to the Jinsha River via the Haikou River before a dam at an elevation of

167 ~1540 m a.s.l. was constructed on its southern side at ~0.3 cal ka BP (Wang and Dou,  
168 1998). The annual mean lake surface temperature (LST) is ~16 °C (Wan et al., 2005).  
169 In summer, the lake becomes thermally stratified, with the thermocline at between 10  
170 to 20 m (Fig. 1C, Lu, 2018). Despite a relatively large catchment, the lake level is  
171 mainly maintained by direct precipitation and groundwater, with a total dissolved  
172 solid load of ~1‰ and pH of ~8 (Wan et al., 2005). The lake is eutrophic with a total  
173 phosphate concentration of 0.05 mg/L, and total nitrogen concentration of 0.89 mg/L  
174 (Li et al., 2019). Topsoil types are lateritic red earths and mountain red brown soils in  
175 the catchment (Wang and Dou, 1998). The Lake Chenghai region is mainly affected  
176 by a warm-humid monsoonal airflow from the tropical Indian Ocean from June to  
177 September, and by the southern branch of the Northern Hemisphere westerly jet  
178 between October and May (Wang and Dou, 1998). The mean annual air temperature  
179 (MAAT) is ~14 °C, the mean annual precipitation is ~660 mm with 80% falling  
180 between June and September (the Yongsheng meteorological station 26.68°N,  
181 100.75°E; elevation of 2130 m a.s.l.).

## 182 2.2. *Sampling and dating*

183 In summer 2016, an 874-cm-long sediment core (CH2016) was retrieved using a  
184 UWITEC coring platform system with a percussion corer in 30 m of water depth  
185 (26°33'29.4"N, 100°39'6.7"E). Each section of the core was split lengthways,  
186 photographed and then sectioned at a 1-cm interval in the laboratory; the samples  
187 stored at 4 °C until analysis. The chronology was established using accelerator mass  
188 spectrometry (AMS) <sup>14</sup>C dating of eight terrestrial plant macrofossils and charcoal  
189 (Sun et al., 2019). The radiocarbon analyses were performed at the Beta Analytic  
190 Radiocarbon Dating Laboratory in Miami, USA. The age model was developed  
191 utilizing Bacon, implemented in R 3.1.0 at 5-cm intervals (Blaauw and Andres  
192 Christen, 2011; R Development Core Team, 2013). All AMS <sup>14</sup>C dates were calibrated  
193 to calendar years before present (0 BP =1950) using the program Calib 7.1 and the  
194 IntCal13 calibration data set (Reimer et al., 2013). The basal mean weighted age is  
195 ~15.6 cal ka BP (Fig. 2, Sun et al., 2019).



196 2.3. Lipid extraction and analysis

197 A total of 102 freeze-dried samples at 4-cm interval were collected for GDGT  
198 analysis over the last deglaciation-Holocene transition. The sampling resolution was  
199 increased to 1-cm between 792- 806 cm, due to the low sedimentation rate observed  
200 in this section. In addition, seven surface (the top 2 cm) sediments covering the whole  
201 lake sampled in 2014 were also analyzed. Lipid extraction was undertaken according  
202 to the procedures in Feng et al (2019). A ~4 g aliquot of each sample was extracted  
203 ultrasonically (4 times) with a mixture of dichloromethane and methanol (9:1, v/v).  
204 The supernatants were condensed and saponified at room temperature for 12 h with a  
205 1 M KOH/methanol solution. The neutral fractions were then separated into apolar  
206 and polar fractions on a silica gel column, using *n*-hexane and methanol, respectively.  
207 The polar fraction containing the GDGTs was concentrated and filtered through 0.45  
208  $\mu\text{m}$  polytetrafluoroethylene syringe filters using *n*-hexane/ isopropanol (99:1 v/v), and  
209 then dried under  $\text{N}_2$ .

210 GDGTs were analyzed using an Agilent 1260 series high performance liquid  
211 chromatography-atmospheric pressure chemical ionization-mass spectrometer  
212 (HPLC-APCI-MS), following the procedure of Yang et al. (2015) at the Institute of  
213 Tibetan Plateau Research, Chinese Academy of Sciences. Briefly, the GDGTs were  
214 separated using three silica columns in tandem (100 mm $\times$  2.1 mm, 1.9  $\mu\text{m}$ ; Thermo  
215 Fisher Scientific, U.S.A.), maintained at 40  $^\circ\text{C}$ . The elution gradients were 84%  
216 *n*-hexane (A): 16% ethyl acetate (B) for 5 min, 84/16 to 82/18 A/B for another 60 min,  
217 then to 100% B for 21 min and kept for 4 min, followed by a return to 84/16 A/B for  
218 30 min. The total flow rate of pump A and pump B was maintained at 0.2 ml/min. The  
219 APCI-MS conditions were: vaporizer pressure 60 psi, vaporizer temperature 400  $^\circ\text{C}$ ,  
220 drying gas flow 6 L/min and temperature 200  $^\circ\text{C}$ , capillary voltage 3500 V and corona  
221 current 5  $\mu\text{A}$  (~3200 V). Selected ion monitoring (SIM) mode was performed to target  
222 specific *m/z* values for each GDGT compound, including 1302 (GDGT-0), 1300  
223 (GDGT-1), 1298 (GDGT-2), 1296 (GDGT-3), and 1292 (crenarchaeol and  
224 crenarchaeol'). The results are presented as the fractional of the sum of the isoGDGTs

225 based on the integration of the peak areas of the [M+H]<sup>+</sup> ions.

#### 226 2.4. Index calculation and temperature reconstruction

227 The percentage of each isoGDGT (X) was calculated according to the following  
228 equation:

$$229 \quad \%X = \frac{X}{(\text{GDGT-0} + \text{GDGT-1} + \text{GDGT-2} + \text{GDGT-3} + \text{crenarchaeol} + \text{crenarchaeol}')} \quad (1)$$

231 The TEX<sub>86</sub> index was defined by Schouten et al. (2002) as follows:

$$232 \quad \text{TEX}_{86} = \frac{(\text{GDGT-2} + \text{GDGT-3} + \text{crenarchaeol}')}{(\text{GDGT-1} + \text{GDGT-2} + \text{GDGT-3} + \text{crenarchaeol}')} \quad (2)$$

234 TEX<sub>86</sub>-inferred LST was calculated using the global lake calibration of  
235 Castañeda and Schouten (2015):

$$236 \quad \text{LST} = 49.03 \times \text{TEX}_{86} - 10.99 \quad (r^2 = 0.88, n=16, \text{RMSE} = 3.1 \text{ } ^\circ\text{C}) \quad (3)$$

237

### 238 3. Results

239 The isoGDGT compositions varied greatly in Lake Chenghai sediments. As  
240 illustrated in Fig. 3, GDGT-0 is the most abundant isoGDGT composition of the  
241 surface sediments. The relative abundance of GDGT-0 (%GDGT-0) ranged from 72.6-  
242 94.4 with a mean of 89.3%, the %cren values varied from 3.8- 18.4% with a mean of  
243 7.7%. The ratios of GDGT-0/crenarchaeol were from 4.0-24.5 with a mean of 15.5.  
244 The average values of GDGT-1, GDGT-2 and GDGT-3 relative abundance were 1.2,  
245 1.1 and 0.7%, respectively. The ~~crenarchaeol's regioisomer,~~ crenarchaeol', occurred in  
246 only low abundance, close to the detection limit, and therefore TEX<sub>86</sub> values could  
247 not be calculated for these surface sediments.

248 The %cren values ranged between 2.4-61.3% with a mean of 52.4% in the core  
249 CH2016. The %cren values were relatively low and highly variable during 15.4-14.4  
250 cal ka BP, ranging between 1.8-32.0%, with a mean of 11.6%. By contrast, the values

251 were relatively stable during 14.4-7.0 cal ka BP, ranging between 41.8-61.3% with a  
252 mean of 58.3%. The relative abundances of crenarchaeol' had a mean of 1.7%. The  
253 ratios of crenarchaeol'/crenarchaeol were highly variable during 15.4-14.4 cal ka BP  
254 with a mean of 0.07. After this time, the values gradually decrease during 14.4-11.7  
255 cal ka BP time interval with a minor increase between 12.5-11.7 cal ka BP, where the  
256 ratio averaged 0.05. The crenarchaeol'/crenarchaeol ratios were generally stable and  
257 fluctuated around 0.03 during the period 11.8-7.0 cal ka BP.

258 The relative abundances of GDGT-0 (%GDGT-0) showed a significant negative  
259 correlation with the %cren in the core CH2016 ( $r= 0.99, p< 0.001$ ). The %GDGT-0  
260 values had a mean of 74.0% between 15.4-14.4 cal ka BP and a mean of 19.6% during  
261 the 14.4-7.0 cal ka BP interval. The values of GDGT-0/crenarchaeol were  
262 generally  $>2$  during the period 15.4-14.4 cal ka BP, ranging from 1.4-49.9 with a  
263 mean of 16.7, and all  $<2$  from 14.4-7.0 cal ka BP. The relative abundance of GDGT-1,  
264 GDGT-2 and GDGT-3 were generally low in the sediments, with means of 8.9, 9.2,  
265 and 1.3, respectively.

266 The  $TEX_{86}$  values were also highly variable during 15.4-14.4 cal ka BP period,  
267 ranging between 0.36-0.68 with a mean of 0.54. Thereafter, the values generally  
268 followed an increasing trend, ranging between 0.49-0.63 with a mean of 0.58.

269

## 270 **4. Discussion**

### 271 *4.1. Provenance of isoGDGTs*

272 In order to evaluate the potential sources of isoGDGTs in Lake Chenghai  
273 sediments, we plotted a ternary diagram to compare the distribution patterns of  
274 GDGT-0, crenarchaeol, and the sum of GDGT-1, GDGT-2, GDGT-3, and  
275 crenarchaeol' (' $TEX_{86}$ ' GDGT) among our samples, previously published Chinese  
276 soils and global marine sediments compiled by Yao et al. (2019), along with  
277 previously published Chinese lacustrine surface sediments results (Günther et al.,  
278 2014; Dang et al., 2016; Hu et al., 2016; Li et al., 2016, 2019; Yao et al., 2019; Wang

279 et al., 2020). In Lake Chenghai surface sediments, GDGT-0 is the predominant  
280 component among the isoGDGTs, consistent with most previous studies of lacustrine  
281 sediments (Blaga et al., 2009; Dang et al., 2016; Li et al., 2019; Yao et al., 2019;  
282 Wang et al., 2020). For example, GDGT-0 can account for more than 90% of total  
283 isoGDGTs in shallow lake surface sediments from East China (Dang et al., 2016); ~80%  
284 in saline pond surface sediments from northeast China (Li et al., 2019), and ~54% in  
285 surface sediments from the Qinghai-Tibetan Plateau (Wang et al., 2020). The values  
286 of GDGT-0/cren >2 in Lake Chenghai surface sediment suggest non-thaumarchaeotal  
287 isoGDGTs are also likely to be an important source in this lake system. The  
288 distribution of isoGDGTs between Chinese lacustrine surface sediments and soils  
289 were similar, and both were generally higher than that in global marine sediments and  
290 Thaumarchaeota. This line of evidence also suggests that the surface sediments could  
291 contain a significant contribution of soil isoGDGTs input (Li et al., 2016; Li et al.,  
292 2019).

293 The distribution of isoGDGT in Lake Chenghai sediment from 15.4-14.4 cal ka  
294 BP was similar to that of the surface sediments, suggesting a substantial contribution  
295 of non-thaumarchaeota during this period. However, the relative abundance of  
296 GDGT-0 significantly decreased and %cren increased in Lake Chenghai sediments  
297 from 14.4-7.0 cal ka BP. The plots generally overlapped with those of global marine  
298 sediments and Thaumarchaeota in the ternary diagram during this period, indicating  
299 that Thaumarchaeota dominated the archaea community in Lake Chenghai during the  
300 late glacial period and the early Holocene. The observed down-core changes in  
301 crenarchaeol'/crenarchaeol ratios may be due to relatively high contributions of group  
302 I.1b Thaumarchaeota from soils during the period 15.4-11.8 cal ka BP, and that these  
303 dominate the contributions of isoGDGTs derived from aquatic group I.1a  
304 Thaumarchaeota during the period from 11.8-7.0 cal ka BP.

#### 305 4.2. Assessment of isoGDGT-based lake-level proxy

306 The environmental ~~implication-interpretation~~ of %cren at Lake Chenghai during  
307 the period from the last deglaciation to the early Holocene is illustrated in Fig. 5.

308 Thaumarchaeota thrive predominantly near the oxycline in stratified lakes, and are  
309 mainly suppressed by non-thaumarchaeotal archaea when the lake level is low (Wang  
310 et al., 2014a; Wang et al., 2017a; Wang et al., 2019). Thus, the abrupt increase  
311 in %cren values is interpreted to represent an increase in lake depth in Lake Chenghai,  
312 from a lowstand during 15.4-14.4 cal ka BP, to a highstand period thereafter. The  
313 relatively low %cren values during 15.4-14.4 cal ka BP is consistent in timing with  
314 the  $\delta^{18}\text{O}$  record of authigenic carbonates derived from the same core (Fig. 4e, Sun et  
315 al., 2019), speleothem  $\delta^{18}\text{O}$  records from Mawmluh Cave and Bittoo Cave in north  
316 India (Fig. 4f, Dutt et al., 2015; Kathayat et al., 2016), and Donnge Cave in southwest  
317 China (Dykoski et al., 2005), which all record a substantial positive shift in  $\delta^{18}\text{O}$   
318 values at that time. Speleothem  $\delta^{18}\text{O}$  records in the ISM region are used as a rainfall  
319 amount proxy, with low  $\delta^{18}\text{O}$  values indicating tracking changes in monsoon  
320 intensityhigh precipitation (Dykoski et al., 2005; Cheng et al., 2012; Dutt et al., 2015).  
321 ~~This suggests that the Thaumarchaeota were mainly suppressed by~~  
322 ~~non-thaumarchaeotal archaea. Thus the abrupt increase in %cren values at 14.4 cal ka~~  
323 ~~BP is suggested to represent a lowstand of Lake Chenghai during 15.4-14.4 cal ka BP,~~  
324 ~~and a highstand period thereafter.~~

325 ~~The interpretation of %cren contradicts the case for Lake Challa, but is~~  
326 ~~consistent with that for Lake Qinghai in northwest China (Sinninghe Damsté et al.,~~  
327 ~~2012; Wang et al., 2014). This difference is possibly due to the different response of~~  
328 ~~Thaumarchaeota in the two types of lakes because of the mixing regime. For the small~~  
329 ~~and deep Lake Challa, there is never complete mixing due to the stable stratification~~  
330 ~~of the warmer water column and the lack of seasonality (Sinninghe Damsté et al.,~~  
331 ~~2009). Below the oxycline nitrate levels are high, more substantial mixing regenerates~~  
332 ~~more nutrients to the surface waters, resulting a relatively higher production of~~  
333 ~~crenarchaeol (Sinninghe Damsté et al., 2012). In contrast, Lake Chenghai and Lake~~  
334 ~~Qinghai are seasonal mixing lakes, and the vertical change of nutrients may be~~  
335 ~~relatively small in the lake water. In addition, the low lake level during the HI event~~  
336 ~~was associated with a weakened ISM, and less terrestrial nutrient input due to less~~

337 ~~runoff would likely suppress the growth of Thaumarchaeota and reduce the~~  
338 ~~production of crenarchaeol.~~

339 Low lake-levels and a weakened ISM during the H1 cold event are also  
340 observed in several previous paleolimnological studies from the Yunnan Plateau, within  
341 the uncertainties of the age model. Diatom and grain-size records from Lake  
342 Tengchongqinghai show a significant decrease in acidophilous diatom species and an  
343 increase in the grain-size of mineral particles from 18.5 to 15.0 cal ka BP, suggesting  
344 that the climate was dry and the ISM was at its weakest since the last deglaciation  
345 (Fig. 4g, Zhang et al., 2017b; Li et al., 2018). Similarly, an increase in >30  $\mu\text{m}$   
346 grain-size particles in the late glacial sediments from Lake Xingyun reflects a period  
347 of abrupt weakening of the ISM during the H1 cold event because of reduced lake  
348 level (Wu et al., 2015). In Lake Lugu, the loss of the planktonic diatoms and a switch  
349 to small *Fragilaria* spp. suggests a weaker stratification from 24.5 to 14.5 cal ka BP,  
350 which might also correspond to low lake-level at that time (Wang et al., 2014b). ~~In~~  
351 ~~addition, there is a peak of cren% centered at ~15.2 cal ka BP, suggesting a centennial~~  
352 ~~high lake level and strengthened ISM period, which was not identified in a previous~~  
353  ~~$\delta^{18}\text{O}$  record of authigenic carbonates (Sun et al., 2019). However, the strengthened~~  
354 ~~ISM event at ~15.2 cal ka BP was clearly recorded by speleothem  $\delta^{18}\text{O}$  record from~~  
355 ~~Dongge Cave in southwest China (Dykoski et al., 2005).~~

356 Lake levels inferred from %cren do not show a lowstand during the YD  
357 (~12.8-11.7 cal ka BP), which is generally recognised as a period of low rainfall due  
358 to the weakening of the ISM (Dutt et al., 2015; Dykoski et al., 2005; Kathayat et al.,  
359 2016; Sun et al., 2019). In contrast, a low lake-level signal is observed in the  $\delta^{18}\text{O}$   
360 record of authigenic carbonates from Lake Chenghai (Sun et al., 2019). ~~In addition,~~  
361 ~~increased~~ Increased lake water alkalinity and decreased lake-level are also recorded  
362 in the diatom and grain-size proxy records between 12.8-11.1 cal ka BP of Lake  
363 Tengchongqinghai (Fig. 4g, Zhang et al., 2017b; Li et al., 2018). In addition, there is a  
364 peak of %cren centered at ~15.2 cal ka BP, suggesting a centennial scale high lake  
365 level and strengthened ISM period, which was not identified in a previous  $\delta^{18}\text{O}$  record

366 | of authigenic carbonates (Sun et al., 2019). The inferred high lake levels during the  
367 | YD and at ~15.2 cal ka BP, which ~~is-are~~ inconsistent with ~~a~~-weakened ISM inferred  
368 | from other proxies, might be due to the erosion of soil organic matter into the lake  
369 | during ~~this~~-these periods (Wang et al., 2019). The crenarchaeol are relatively abundant  
370 | in topsoils from southwest China, and the influence of soil input should be more  
371 | significant at times of drier conditions (Yang et al., 2019). It is also worth noting that  
372 | the crenarchaeol<sup>7</sup>/crenarchaeol ratios were not only relatively higher during the H1  
373 | cold event, but also showed a minor reversal during the YD cold event. These results  
374 | are consistent with group I.1b Thaumarchaeota being an important source of  
375 | isoGDGTs in small lakes and in the nearshore areas of large lakes (Wang et al., 2019).

376 | Another possibility for the ~~unexpected-different~~ H1 and YD lake level variation  
377 | is the sensitivity of the proxy to lake-level ~~variation~~ in the case of Lake Chenghai.  
378 | The  $\delta^{18}\text{O}$  record of authigenic carbonates from Lake Chenghai and speleothem  $\delta^{18}\text{O}$   
379 | records in the ISM region suggest that the weakening of the ISM during the YD was  
380 | less marked than that occurring during the H1 event, in turn suggesting that  
381 | lake-levels in southwest China may have been higher during the YD than the H1  
382 | event (Dykoski et al., 2005; Dutt et al., 2015; Kathayat et al., 2016; Sun et al., 2019;  
383 | Zhang et al., 2019). For the %cren proxy, we note that the values are correlated to the  
384 | logarithm of depth, suggesting that %cren may be less sensitive to water depth  
385 | variation when the lake-level is relatively high, and more sensitive to water depth  
386 | variation when the lake-level is lower (Wang et al., 2019).

387 | The interpretation of %cren presented here differs from that proposed for Lake  
388 | Challa, but is consistent with that proposed for Lake Qinghai in northwest China  
389 | (Sinninghe Damst  t et al., 2012a; Wang et al., 2014). This difference is possibly due to  
390 | the different response of Thaumarchaeota in the two types of lakes because of the  
391 | different mixing regime. For the small and deep Lake Challa, there is never complete  
392 | mixing due to the stable stratification of the warmer water column and a lack of  
393 | seasonality (Sinninghe Damst  t et al., 2009). Below the oxycline nitrate levels are high,  
394 | so more substantial mixing regenerates more nutrients into the surface waters.

395 resulting a relatively higher production of crenarchaeol when lake level is  
396 substantially reduced (Sinninghe Damsté et al., 2012a). In contrast, Lake Chenghai  
397 and Lake Qinghai are seasonally mixed lakes, and the vertical change in nutrients may  
398 be relatively small. In addition, terrestrial nutrient input would be a shorter time-scale  
399 mechanism explaining the relationship between ISM index and %cren values (Wang  
400 et al., 2014). Less nutrient input due to a weakened ISM during the HI event would  
401 likely suppress the growth of Thaumarchaeota and reduce the production of  
402 crenarchaeol.

#### 403 4.3. Warming in the last deglaciation-Holocene transition

404 The application of the TEX<sub>86</sub>-based paleotemperature calibration depends  
405 critically on the assumption that the isoGDGTs used for calculation of TEX<sub>86</sub> values  
406 are mainly been derived from group I.1a in the water column (Blaga et al., 2009;  
407 Castañeda and Schouten, 2011; Powers et al., 2010; Sinninghe Damsté et al., 2012a).  
408 Since the influence of methanogenic archaea in the water column or archaea in the  
409 catchment soils has been recognized as significant, Lake Chenghai sediments with  
410 crenarchaeol'/crenarchaeol ratios >0.04 and/or GDGT-0/crenarchaeol ratio >2 are  
411 excluded from the discussion below (Powers et al., 2010; Castañeda and Schouten,  
412 2015). The ratio of branched GDGTs to isoGDGTs (BIT) should be <0.5 if the  
413 TEX<sub>86</sub>-temperature calibration in previous studies, because the values are  
414 generally >0.90 in soils, whereas values are close to zero for sediments from large  
415 lakes (Hopmans et al., 2004; Weijers et al., 2006). However, recent studies of a wide  
416 variety of lakes have suggested that at least some of the branched GDGTs can be  
417 produced *in situ* in the lake (Blaga et al., 2010; Tierney et al., 2010; Pearson et al.,  
418 2011; Hu et al., 2016; Dang et al., 2018; Russell et al., 2018). Therefore, *in situ*  
419 production of branched GDGTs in Lake Chenghai cannot be fully excluded, and  
420 therefore the ratio of ~~branched GDGTs to isoGDGTs~~BIT was ignored in this study. 74  
421 samples remain that have isoGDGT distributions consistent with their dominant  
422 source being the aquatic Thaumarchaeota, most of these being from the time interval  
423 between 11.7-7.0 cal ka BP, and only a few from the last deglaciation (n= 6). Using



424 Equation 4 developed by Castañeda and Schouten (2015) to calculate mean LST,  
425 yielded LST values from 14.3-20.1 °C, with a mean of 18.0 °C (Fig. 5a).

426 LST was ~15.9 °C during the last deglacial period, a temperature approaching  
427 the 16 °C observed in the present Lake Chenghai. ~~Considering the TEX<sub>86</sub>-based~~  
428 LST transfer function has a RMSE of 3.1 °C, this result is consistent with other recent  
429 reconstructed ~~mean annual temperatures (MAAT)~~ in southwest China, which show  
430 the temperatures during the last deglaciation were generally similar to the present-day  
431 values. For example, the MAAT inferred from branched GDGTs from Lake  
432 Tengchongqinghai in southwest China increased episodically from 12.0 °C to 14.0 °C  
433 between 19.2 and 10.0 cal ka BP, where the modern mean annual temperature is  
434 14.7 °C (Tian et al., 2019). The TEX<sub>86</sub>-based deglacial LST and MAAT inferred from  
435 branched GDGTs from Nam Co in south Tibetan Plateau also reported values similar  
436 to the present-day (Günther et al., 2015). ~~Furthermore~~In contrast, the July air  
437 temperature derived from the chironomid record from Lake Tiancai, and pollen record  
438 from Lake Yidun showed that the climate during the deglacial period was ~2-3 °C  
439 cooler relative to today (Fig. 5b and c, Shen et al., 2006; Zhang et al., 2019). The  
440 amplitudes of reconstructed terrestrial temperatures change in the Indian summer  
441 monsoon region are generally consistent with those from the tropical Indian Ocean.  
442 Although estimates of sea surface temperatures in the Andaman Sea and Bay of  
443 Bengal were variable, the cooling relative to today ranged from 1-4 °C (Rashid et al.,  
444 2007; MARGO, 2009; Govil and Naidu, 2011; Gebregiorgis et al., 2016).

445 Following the YD cold event, LST at Lake Chenghai ranged from 16.2 °C to  
446 20.1 °C with an increasing trend, and the middle Holocene was generally warmer than  
447 the early Holocene (11.7- 8.2 cal ka BP). In the Indian summer monsoon region, the  
448 reconstructed MAAT using the branched GDGT calibration from Lake  
449 Ximenglongtan remained at ~12.5 °C from 9.4-7.6 cal ka BP, then experienced a rapid  
450 warming to 13.8 °C from 7.6-5.5 cal ka BP (Ning et al., 2019). Meanwhile, the  
451 branched GDGTs-MAAT from Lake Tengchongqinghai also achieved its highest the  
452 highest value at around 7.1 cal ka BP (Tian et al., 2019). Similarly, summer air

453 temperatures reconstructed from Lake Tiancai and Lake Xingyun displayed ~~lower~~  
454 ~~values in a warming trend from~~ the early Holocene to the mid-Holocene ~~when~~  
455 ~~compared with that in the following millennium, though the amplitude of change is~~  
456 ~~much lower (0.3 and 1.1 °C lower, respectively, Zhang et al., 2017a; Wu et al., 2018).~~  
457 The amplitude of the absolute scale of ~~cooling and~~ warming is of a lower magnitude  
458 in the chironomid, pollen and branched GDGT records as compared to the  
459 TEX<sub>86</sub>-based reconstruction from Lake Chenghai. This may be due to the difference  
460 in the accuracy and precision of the proxy-based models, which also depend on the  
461 biological and seasonal sensitivity of the proxy, to constrain the absolute temperature  
462 values (Zhang et al., 2017a).

463 We also noted that most of the lake records from not only the Indian summer  
464 monsoon region, but other parts of ~~East~~-Asia, show a ~~thermal optimum at warming~~  
465 ~~from 8.0-11.7-7.0 cal ka BP~~ (Ning et al., 2019). In southwest China, Holocene summer  
466 air temperature generally follows ~~The~~ summer insolation over the Northern  
467 Hemisphere, ~~which is an important external forcing, was~~ but lags the highest value at  
468 ~~~11.0 cal ka BP, leading the temperature optimum in east and south Asia~~ by 3-4 ka  
469 (Berger and Loutre, 1991; Zhang et al., 2017a; Wu et al., 2018). This indicates that  
470 additional feedback between solar insolation and internal processes, such as the  
471 persistence of remnants of the Northern Hemisphere ice-sheets and snow cover during  
472 the early Holocene, should be considered in explaining this discrepancy (Zhang et al.,  
473 2017a, Wu et al., 2018; Ning et al., 2019). This is evidenced by records from the  
474 Laurentide ice-sheets, which were still relatively large at ~11 cal ka BP, despite the  
475 occurrence of peak summer insolation (Shuman et al., 2005). The Laurentide and  
476 Fennoscandian ice sheets in the early Holocene enhanced surface albedo and reduced  
477 air temperature in the high latitudes, which likely led to enhanced westerlies  
478 transporting more cold air from the North Atlantic Ocean downward to the Indian  
479 monsoon-affected regions of southwest China and north India through its south branch  
480 flow (Ning et al., 2019). In addition, ~~†~~ The melting of ice-sheets from 11-6 cal ka BP is  
481 likely to have slowed down the Atlantic Meridional Overturning Circulation and

482 impeded the northward shift of the Intertropical Convergence Zone (Dykoski et al.,  
483 2005). This process could further result in a relatively weakened Indian summer  
484 monsoon, and a reduction in heat transported to the continent during the early  
485 Holocene (Zhang et al., 2017a). In addition, the ice-sheets in the early Holocene  
486 enhanced surface albedo and reduced air temperature in the high latitudes, which  
487 likely led to enhanced westerlies transporting more cold air from the North Atlantic  
488 Ocean downward to the ISM affected regions through its south branch flow,  
489 especially during the winter (Ning et al., 2019). A long-term winter warming trend in  
490 southwest China was revealed by the pollen record from Lake Wuxu and Muge from  
491 the southeast margin of the Qinghai-Tibetan Plateau (Zhang et al., 2016; Ni et al.,  
492 2019). In the high latitudes of the Northern Hemisphere, the early Holocene winter  
493 warming is attributed to increasing winter insolation, as well as the retreat of the  
494 Northern Hemisphere ice-sheets (Baker et al., 2017; Marsicek et al., 2018). Although  
495 our LST record from Lake Chenghai has not been determined to be an indicator of  
496 summer or winter temperature, it does appear that long-term temperature evolution  
497 during the early Holocene to the mid-Holocene, which was driven mainly by solar  
498 insolation and the status of Northern Hemisphere ice-sheets. In essence, more  
499 temperature records with unambiguous seasonal significance from different regions  
500 are needed to achieve a comprehensive understanding of Holocene temperature  
501 dynamics.

## 503 **5. Conclusions**

504 The record of isoGDGTs in the sediments of Lake Chenghai in southwest China  
505 presented in this study allows us to test the ability of isoGDGT-based proxies in the  
506 ISM region to reconstruct lake-level and temperature during the last  
507 deglaciation-Holocene transition. The lake-level history inferred from %cren shows a  
508 relative lowstand of Lake Chenghai during 15.4-14.4 cal ka BP, corresponding to a  
509 period of weakened ISM during the H1 cold event. The indistinct signal of lake-level  
510 variation during the YD cold event may be due to the group I.1b Thaumarchaeota

511 being an important source of isoGDGTs and consequently the lake level may have  
512 been low during the YD cold event. After filtering for the influence of isoGDGTs  
513 derived from soils in the surrounding catchment and non-thaumarchaeota, the TEX<sub>86</sub>  
514 paleothermometry revealed that the LST of Lake Chenghai was similar to the  
515 present-day value during the last deglaciation. The lake also experienced a substantial  
516 warming of ~4 °C from the early-Holocene to the mid-Holocene due to the melting of  
517 the remnants of the continental ice-sheets in the Northern Hemisphere, which  
518 gradually enhanced the ISM and reduced the winter westerly circulation. Overall, our  
519 results show that records of isoGDGTs in Lake Chenghai sediments have potential for  
520 quantitative paleotemperature reconstruction once potential underlying biases are  
521 properly constrained.

522

#### 523 **Data availability.**

524 All data generated in this study can be found in the Supplement.~~All data in this study~~  
525 ~~will be made available on request.~~

#### 526 **Author contributions.**

527 W.S and E.Z designed the study, W.S performed the fieldwork and lab analysis. W.S  
528 and E.Z led the writing of the paper, J.C, J. S, M.I.B, C.Z, Q.J and J.S contributed to  
529 data interpretation and paper writing. All authors contributed to discussions and  
530 writing of the manuscript. The authors declare that they have no competing financial  
531 interests.

#### 532 **Competing interests.**

533 The authors declare that they have no conflict of interest.

#### 534 **Acknowledgments.**

535 We would like to thank two anonymous reviewers for their valuable suggestion on  
536 this article, as well as~~We thank~~ Dr. R. Chen and D. Ning for field assistance and  
537 laboratory analysis.

538 **Financial support.**

539 The research was supported by the found from the program of Global Change and  
540 Mitigation (2016YFA0600502), the National Natural Science Foundation of China  
541 (41702183 and 41572337), the Strategic Priority Research Program of Chinese  
542 Academy of Sciences (XDB40010200), and the fund from State Key Laboratory of  
543 Lake Science and Environment (2016SKL003).

544

545 **References**

546 Alley, R.B., Clark, P.U.: The deglaciation of the northern hemisphere: A global  
547 perspective. *Annu. Rev. Earth Pl. Sc.* 27, 149-182, DOI:  
548 10.1146/annurev.earth.27.1.149, 1999.

549 Baker, J.L., Lachniet, M.S., Chervyatsova, O., Asmerom, Y., Polyak, V.J.: Holocene  
550 warming in western continental Eurasia driven by glacial retreat and greenhouse  
551 forcing. *Nature Geosci.* 10, 430-435, DOI: 10.1038/ngeo2953, 2017.

552 Berger, A., Loutre, M.-F.: Insolation values for the climate of the last 10 million years.  
553 *Quaternary. Sci. Rev.* 10, 297-317: DOI: 10.1016/0277-3791(91)90033-Q, 1991.

554 Berke, M.A., Johnson, T.C., Werne, J.P., Schouten, S., Sinninghe Damst é J.S.: A  
555 mid-Holocene thermal maximum at the end of the African Humid Period. *Earth.*  
556 *Planet. Sc. Lett.* 351-352, 95-104, DOI: 10.1016/j.epsl.2012.07.008, 2012.

557 Blaauw, M., Andres Christen, J.: Flexible paleoclimate age-depth models using an  
558 autoregressive gamma process. *Bayesian. Anal.* 6, 457-474,  
559 DOI: 10.1214/11-BA618, 2011.

560 Blaga, C.I., Reichart, G.-J., Heiri, O., Sinninghe Damst é J.S.: Tetraether membrane  
561 lipid distributions in water-column particulate matter and sediments: a study of  
562 47 European lakes along a north–south transect. *J. Paleolimnol.* 41, 523-540,  
563 DOI: 10.1007/s10933-008-9242-2, 2009.

564 Blaga, C.I., Reichart, G.-J., Lotter, A.F., Anselmetti, F.S., Sinninghe Damst é J.S.: A  
565 TEX<sub>86</sub> lake record suggests simultaneous shifts in temperature in Central Europe  
566 and Greenland during the last deglaciation. *Geophys. Res. Lett.* 40, 948-953,

567 DOI: 10.1002/grl.50181, 2013.

568 Blaga, C.I., Reichart, G.-J., Vissers, E.W., Lotter, A.F., Anselmetti, F.S., Sinninghe  
569 Damsté J.S.: Seasonal changes in glycerol dialkyl glycerol tetraether  
570 concentrations and fluxes in a perialpine lake: Implications for the use of the  
571 TEX86 and BIT proxies. *Geochim. Cosmochim. Ac.* 75, 6416-6428, DOI:  
572 10.1016/j.gca.2011.08.016, 2011.

573 Blaga, C.I., Reichart, G.J., Schouten, S., Lotter, A.F., Werne, J.P., Kosten, S., Mazzeo,  
574 N., Lacerot, G., Damste, J.S.S.: Branched glycerol dialkyl glycerol tetraethers in  
575 lake sediments: Can they be used as temperature and pH proxies? *Org. Geochem.*  
576 41, 1225-1234, DOI: 10.1016/j.orggeochem.2010.07.002, 2010.

577 Buckles, L.K., Villanueva, L., Weijers, J.W.H., Verschuren, D., Damsté J.S.S.:  
578 Linking isoprenoidal GDGT membrane lipid distributions with gene abundances  
579 of ammonia-oxidizing Thaumarchaeota and uncultured crenarchaeotal groups in  
580 the water column of a tropical lake (Lake Challa, East Africa). *Environ. J.*  
581 *Microbiol.* 15, 2445-2462, DOI: 10.1111/1462-2920.12118, 2013.

582 Carlson, A.E., LeGrande, A.N., Oppo, D.W., Came, R.E., Schmidt, G.A., Anslow, F.S.,  
583 Licciardi, J.M., Obbink, E.A.: Rapid early Holocene deglaciation of the  
584 Laurentide ice sheet. *Nature Geosci.* 1, 620-624, DOI: 10.1038/ngeo285, 2008.

585 Castañeda, I.S., Schouten, S.: A review of molecular organic proxies for examining  
586 modern and ancient lacustrine environments. *Quaternary. Sci. Rev.* 30,  
587 2851-2891, DOI: 10.1016/j.quascirev.2011.07.009, 2011.

588 Castañeda, I.S., Schouten, S.: Corrigendum to “A review of molecular organic proxies  
589 for examining modern and ancient lacustrine environments” [*Quat. Sci. Rev.* 30  
590 (2011) 2851–2891]. *Quaternary. Sci. Rev.* 125, 174-176, DOI:  
591 10.1016/j.quascirev.2015.07.020, 2015.

592 Cheng, H., Sinha, A., Wang, X., Cruz, F.W., Edwards, R.L.: The Global  
593 Paleomonsoon as seen through speleothem records from Asia and the Americas.  
594 *Clim. Dynam.* 39, 1045-1062, DOI: 10.1007/s00382-012-1363-7, 2012.

595 Contreras-Rosales, L.A., Jennerjahn, T., Tharammal, T., Meyer, V., Lückge, A., Paul,  
596 A., Schefuß, E.: Evolution of the Indian Summer Monsoon and terrestrial

597 vegetation in the Bengal region during the past 18 ka. *Quaternary. Sci. Rev.* 102,  
598 133-148, DOI: 10.1016/j.quascirev.2014.08.010, 2014.

599 Dang, X., Ding, W., Yang, H., Pancost, R.D., Naafs, B.D.A., Xue, J., Lin, X., Lu, J.,  
600 Xie, S.: Different temperature dependence of the bacterial brGDGT isomers in  
601 35 Chinese lake sediments compared to that in soils. *Org. Geochem.*, DOI:  
602 10.1016/j.orggeochem.2018.02.008, 2018.

603 Dang, X.Y., Xue, J.T., Yang, H., Xie, S.C.: Environmental impacts on the distribution  
604 of microbial tetraether lipids in Chinese lakes with contrasting pH: Implications  
605 for lacustrine paleoenvironmental reconstructions. *Sci. China. Earth. Sci.* 59,  
606 939-950, DOI: 10.1007/s11430-015-5234-z, 2016.

607 Dutt, S., Gupta, A.K., Clemens, S.C., Cheng, H., Singh, R.K., Kathayat, G., Edwards,  
608 R.L.: Abrupt changes in Indian summer monsoon strength during 33,800 to  
609 5500 years B.P. *Geophys. Res. Lett.* 42, 5526-5532, DOI:  
610 10.1002/2015GL064015, 2015.

611 Dykoski, C.A., Edwards, R.L., Cheng, H., Yuan, D., Cai, Y., Zhang, M., Lin, Y., Qing,  
612 J., An, Z., Revenaugh, J.: A high-resolution, absolute-dated Holocene and  
613 deglacial Asian monsoon record from Dongge Cave, China. *Earth. Planet. Sc.*  
614 *Lett.* 233, 71-86, DOI: 10.1016/j.epsl.2005.01.036, 2005.

615 Feng, X., Zhao, C., D'Andrea, W.J., Liang, J., Zhou, A., Shen, J.: Temperature  
616 fluctuations during the Common Era in subtropical southwestern China inferred  
617 from brGDGTs in a remote alpine lake. *Earth. Planet. Sc. Lett.* 510, 26-36, DOI:  
618 10.1016/j.epsl.2018.12.028, 2019.

619 Filippi, M.L., Talbot, M.R.: The palaeolimnology of northern Lake Malawi over the  
620 last 25 ka based upon the elemental and stable isotopic composition of  
621 sedimentary organic matter. *Quaternary. Sci. Rev.* 24, 1303-1328, DOI:  
622 10.1016/j.quascirev.2004.10.009, 2005.

623 Gebregiorgis, D., Hathorne, E.C., Sijinkumar, A.V., Nath, B.N., Nürnberg, D., Frank,  
624 M.: South Asian summer monsoon variability during the last ~54 kyrs inferred  
625 from surface water salinity and river runoff proxies. *Quaternary. Sci. Rev.* 138,  
626 6-15, DOI: 10.1016/j.quascirev.2016.02.012, 2016.

627 Govil, P., Divakar Naidu, P.: Variations of Indian monsoon precipitation during the  
628 last 32 kyr reflected in the surface hydrography of the Western Bay of Bengal.  
629 Quaternary. Sci. Rev. 30, 3871-3879, DOI: 10.1016/j.quascirev.2011.10.004,  
630 2011.

631 Günther, F., Thiele, A., Gleixner, G., Xu, B., Yao, T., Schouten, S.: Distribution of  
632 bacterial and archaeal ether lipids in soils and surface sediments of Tibetan lakes:  
633 Implications for GDGT-based proxies in saline high mountain lakes. Org.  
634 Geochem. 67, 19-30, DOI: 10.1016/j.orggeochem.2013.11.014, 2014.

635 Günther, F., Witt, R., Schouten, S., Mäusbacher, R., Daut, G., Zhu, L., Xu, B., Yao, T.,  
636 Gleixner, G.: Quaternary ecological responses and impacts of the Indian Ocean  
637 Summer Monsoon at Nam Co, Southern Tibetan Plateau. Quaternary. Sci. Rev.  
638 112, 66-77, 10.1016/j.quascirev.2015.01.023, 2015.

639 Hu, J., Zhou, H., Peng, P.a., Spiro, B.: Seasonal variability in concentrations and  
640 fluxes of glycerol dialkyl glycerol tetraethers in Huguangyan Maar Lake, SE  
641 China: Implications for the applicability of the MBT-CBT paleotemperature  
642 proxy in lacustrine settings. Chem. Geol. 420, 200-212, DOI:  
643 10.1016/j.chemgeo.2015.11.008, 2016.

644 Kathayat, G., Cheng, H., Sinha, A., Spöhl, C., Edwards, R.L., Zhang, H., Li, X., Yi, L.,  
645 Ning, Y., Cai, Y., Lui, W.L., Breitenbach, S.F.M.: Indian monsoon variability on  
646 millennial-orbital timescales. Sci. Rep-UK. 6, DOI: 10.1038/srep24374, 2016.

647 Kim, J.-G., Jung, M.-Y., Park, S.-J., Rijpstra, W.I.C., Sinninghe Damsté J.S., Madsen,  
648 E.L., Min, D., Kim, J.-S., Kim, G.-J., Rhee, S.-K.: Cultivation of a highly  
649 enriched ammonia-oxidizing archaeon of thaumarchaeotal group I.1b from an  
650 agricultural soil. Environ. Microbiol. 14, 1528-1543, DOI:  
651 10.1111/j.1462-2920.2012.02740.x, 2012.

652 Kim, J.-H., van der Meer, J., Schouten, S., Helmke, P., Willmott, V., Sangiorgi, F.,  
653 Koç N., Hopmans, E.C., Damsté J.S.S.: New indices and calibrations derived  
654 from the distribution of crenarchaeal isoprenoid tetraether lipids: Implications for  
655 past sea surface temperature reconstructions. Geochim. Cosmochim. Ac. 74,  
656 4639-4654, DOI: 10.1016/j.gca.2010.05.027, 2010.



657 Li, J.J., Pancost, R.D., Naafs, B.D.A., Yang, H., Zhao, C., Xie, S.C.: Distribution of  
658 glycerol dialkyl glycerol tetraether (GDGT) lipids in a hypersaline lake system.  
659 *Org. Geochem.* 99, 113-124, DOI: 10.1016/j.orggeochem.2016.06.007, 2016.

660 Li, J., Pancost, R.D., Naafs, B.D.A., Yang, H., Liu, D., Gong, L., Qiu, X., Xie, S.:  
661 Multiple environmental and ecological controls on archaeal ether lipid  
662 distributions in saline ponds. *Chem. Geol.* 529, 119293: DOI:  
663 10.1016/j.chemgeo.2019.119293, 2019.

664 Li, K., Zhou, Y., Zhou, Q., Dong, Y., Zhang, Y., Chang, J., Chen, L., Lu, Y.:  
665 Temporal-spatial distribution of euphotic depth and its influencing factors in  
666 Lake Chenghai, Yunnan Province, China. *J. Lake Sci.* 31 (1), 256-267, DOI: 10.  
667 18307 /2019. 0124, .2019

668 Li, Y., Chen, X., Xiao, X., Zhang, H., Xue, B., Shen, J., Zhang, E.: Diatom-based  
669 inference of Asian monsoon precipitation from a volcanic lake in southwest  
670 China for the last 18.5 ka. *Quaternary. Sci. Rev.* 182, 109-120, DOI:  
671 10.1016/j.quascirev.2017.11.021, 2018.

672 Ling, Y., Sun, Q., Zheng, M., Wang, H., Luo, Y., Dai, X., Xie, M., Zhu, Q.:  
673 Alkenone-based temperature and climate reconstruction during the last  
674 deglaciation at Lake Dangxiong Co, southwestern Tibetan Plateau. *Quatern. Int.*  
675 443, 58-69, DOI: 10.1016/j.quaint.2016.07.036, 2017.

676 Ljungqvist, F.C., Krusic, P.J., Sundqvist, H.S., Zorita, E., Brattström, G., Frank, D.:  
677 Northern Hemisphere hydroclimate variability over the past twelve centuries.  
678 *Nature* 532, 94-98, DOI: 10.1038/nature17418, 2016.

679 Lu Z., Study on climatic and environmental changes of the Yunnan Chenghai region  
680 recorded bylake sediments since 1800 [D]. Kunming: The master Thesis of  
681 Yunnan Normal University, 39-43, 2018.

682 MARGO Project Members: Constraints on the magnitude and patterns of ocean  
683 cooling at the Last Glacial Maximum. *Nature Geosci.* 2, 127-132, DOI:  
684 10.1038/ngeo411, 2009.

685 [Marsicek, J., Shuman, B.N., Bartlein, P.J., Shafer, S.L., Brewer, S.: Reconciling](#)  
686 [divergent trends and millennial variations in Holocene temperatures. \*Nature\* 554,](#)

687 | [92-96, DOI: 10.1038/nature25464, 2018.](https://doi.org/10.1038/nature25464)

688 | McManus, J.F., Francois, R., Gherardi, J.M., Keigwin, L.D., Brown-Leger, S.:

689 | Collapse and rapid resumption of Atlantic meridional circulation linked to

690 | deglacial climate changes. *Nature* 428, 834-837, DOI: 10.1038/nature02494,

691 | 2004.

692 | Meegan Kumar, D., Woltering, M., Hopmans, E.C., Sinninghe Damsté J.S., Schouten,

693 | S., Werne, J.P.: The vertical distribution of Thaumarchaeota in the water column

694 | of Lake Malawi inferred from core and intact polar tetraether lipids. *Org.*

695 | *Geochem.* 132, 37-49, DOI: 10.1016/j.orggeochem.2019.03.004, 2019.

696 | [Ni, Z., Jones, R., Zhang, E., Chang, J., Shulmeister, J., Sun, W., Wang, Y., Ning, D.:](https://doi.org/10.1016/j.palaeo.2019.06.005)

697 | [Contrasting effects of winter and summer climate on Holocene montane](https://doi.org/10.1016/j.palaeo.2019.06.005)

698 | [vegetation belts evolution in southeastern Qinghai-Tibetan Plateau, China.](https://doi.org/10.1016/j.palaeo.2019.06.005)

699 | [Palaeogeogr. Palaeocl. 533, 109232, DOI: 10.1016/j.palaeo.2019.06.005, 2019.](https://doi.org/10.1016/j.palaeo.2019.06.005)

700 | Ning, D., Zhang, E., Shulmeister, J., Chang, J., Sun, W., Ni, Z.: Holocene mean

701 | annual air temperature (MAAT) reconstruction based on branched glycerol

702 | dialkyl glycerol tetraethers from Lake Ximenglongtan, southwestern China. *Org.*

703 | *Geochem.* 133, 65-76, DOI: 10.1016/j.orggeochem.2019.05.003, 2019.

704 | Pearson, E.J., Juggins, S., Talbot, H.M., Weckstrom, J., Rosen, P., Ryves, D.B.,

705 | Roberts, S.J., Schmidt, R.: A lacustrine GDGT-temperature calibration from the

706 | Scandinavian Arctic to Antarctic: Renewed potential for the application of

707 | GDGT-paleothermometry in lakes. *Geochim. Cosmochim. Ac.* 75, 6225-6238,

708 | DOI: 10.1016/j.gca.2011.07.042, 2011.

709 | Pitcher, A., Hopmans, E.C., Mosier, A.C., Park, S.-J., Rhee, S.-K., Francis, C.A.,

710 | Schouten, S., Sinninghe Damsté J.S.: Core and Intact Polar Glycerol

711 | Dibiphytanyl Glycerol Tetraether Lipids of Ammonia-Oxidizing Archaea

712 | Enriched from Marine and Estuarine Sediments. *Appl. Environ. Microb.* 77,

713 | 3468, DOI: 10.1128/AEM.02758-10, 2011.

714 | Powers, L., Werne, J.P., Vanderwoude, A.J., Sinninghe Damsté J.S., Hopmans, E.C.,

715 | Schouten, S.: Applicability and calibration of the TEX<sub>86</sub> paleothermometer in

716 | lakes. *Org. Geochem.* 41, 404-413, DOI: 10.1016/j.orggeochem.2009.11.009,

717 2010.

718 Powers, L.A., Werne, J.P., Johnson, T.C., Hopmans, E.C., Damsté, J.S.S., Schouten, S.:  
719 Crenarchaeotal membrane lipids in lake sediments: A new paleotemperature  
720 proxy for continental paleoclimate reconstruction? *Geology* 32, 613-616, DOI:  
721 10.1130/G20434.1, 2004.

722 R Development Core Team, R: A language and environment for statistical computing,  
723 R Foundation for Statistical Computing, Vienna, Austria, 2013.

724 Rashid, H., Flower, B.P., Poore, R.Z., Quinn, T.M.: A ~25 ka Indian Ocean monsoon  
725 variability record from the Andaman Sea. *Quaternary. Sci. Rev.* 26, 2586-2597,  
726 DOI: 10.1016/j.quascirev.2007.07.002, 2007.

727 Reimer, P.J., Bard, E., Bayliss, A., Beck, J.W., Blackwell, P.G., Ramsey, C.B., Buck,  
728 C.E., Cheng, H., Edwards, R.L., Friedrich, M.: IntCal13 and Marine13  
729 radiocarbon age calibration curves 0–50,000 years cal BP. *Radiocarbon* 55,  
730 1869-1887, DOI: 10.2458/azu\_js\_rc.55.16947, 2013.

731 Russell, J.M., Hopmans, E.C., Loomis, S.E., Liang, J., Sinninghe Damsté J.S.:  
732 Distributions of 5- and 6-methyl branched glycerol dialkyl glycerol tetraethers  
733 (brGDGTs) in East African lake sediment: Effects of temperature, pH, and new  
734 lacustrine paleotemperature calibrations. *Org. Geochem.* 117, 56-69, DOI:  
735 10.1016/j.orggeochem.2017.12.003, 2018.

736 Saraswat, R., Lea, D.W., Nigam, R., Mackensen, A., Naik, D.K.: Deglaciation in the  
737 tropical Indian Ocean driven by interplay between the regional monsoon and  
738 global teleconnections. *Earth. Planet. Sc. Lett.* 375, 166-175, DOI:  
739 10.1016/j.epsl.2013.05.022, 2013.

740 Schouten, S., Hopmans, E.C., Schefuß, E., Sinninghe Damsté J.S.: Distributional  
741 variations in marine crenarchaeotal membrane lipids: a new tool for  
742 reconstructing ancient sea water temperatures? *Earth. Planet. Sc. Lett.* 204,  
743 265-274, DOI: 10.1016/S0012-821X(02)00979-2, 2002.

744 Schouten, S., Hopmans, E.C., Sinninghe Damsté J.S.: The organic geochemistry of  
745 glycerol dialkyl glycerol tetraether lipids: A review. *Org. Geochem.* 54, 19-61,  
746 DOI: 10.1016/j.orggeochem.2012.09.006, 2013.

747 Schouten, S., Rijpstra, W.I.C., Durisch-Kaiser, E., Schubert, C.J., Sinninghe Damsté  
748 J.S.: Distribution of glycerol dialkyl glycerol tetraether lipids in the water  
749 column of Lake Tanganyika. *Org. Geochem.* 53, 34-37, DOI:  
750 10.1016/j.orggeochem.2012.01.009, 2012.

751 Shen, C., Liu, K.-b., Tang, L., Overpeck, J.T.: Quantitative relationships between  
752 modern pollen rain and climate in the Tibetan Plateau. *Rev. Palaeobot. Palyno.*  
753 140, 61-77, DOI: 10.1016/j.revpalbo.2006.03.001, 2006.

754 [Shuman, B., Bartlein, P.J., Webb, T.: The magnitudes of millennial- and orbital-scale](#)  
755 [climatic change in eastern North America during the Late Quaternary. \*Quaternary\*](#)  
756 [\*Sci. Rev.\* 24, 2194-2206, DOI: 10.1016/j.quascirev.2005.03.018, 2005.](#)

757 Sinha, A., Kathayat, G., Cheng, H., Breitenbach, S.F.M., Berkelhammer, M.,  
758 Mudelsee, M., Biswas, J., Edwards, R.L.: Trends and oscillations in the Indian  
759 summer monsoon rainfall over the last two millennia. *Nat. Commun.* 6, DOI:  
760 10.1038/ncomms7309, 2015.

761 Sinha, A., Stott, L., Berkelhammer, M., Cheng, H., Edwards, R.L., Buckley, B.,  
762 Aldenderfer, M., Mudelsee, M.: A global context for megadroughts in monsoon  
763 Asia during the past millennium. *Quaternary. Sci. Rev.* 30, 47-62, DOI:  
764 10.1016/j.quascirev.2010.10.005, 2011.

765 Sinninghe Damsté J.S., Ossebaar, J., Abbas, B., Schouten, S., Verschuren, D.: Fluxes  
766 and distribution of tetraether lipids in an equatorial African lake: Constraints on  
767 the application of the TEX<sub>86</sub> palaeothermometer and BIT index in lacustrine  
768 settings. *Geochim. Cosmochim. Ac.* 73, 4232-4249, DOI:  
769 10.1016/j.gca.2009.04.022, 2009.

770 Sinninghe Damsté J.S., Ossebaar, J., Schouten, S., Verschuren, D.: Distribution of  
771 tetraether lipids in the 25-ka sedimentary record of Lake Challa: extracting  
772 reliable TEX<sub>86</sub> and MBT/CBT palaeotemperatures from an equatorial African  
773 lake. *Quaternary. Sci. Rev.* 50, 43-54, DOI: 10.1016/j.quascirev.2012.07.001,  
774 2012a.

775 Sinninghe Damsté J.S., Rijpstra, W.I.C., Hopmans, E.C., Jung, M.-Y., Kim, J.-G.,  
776 Rhee, S.-K., Stieglmeier, M., Schleper, C.: Intact Polar and Core Glycerol

777 Dibiphytanyl Glycerol Tetraether Lipids of Group I.1a and I.1b *Thaumarchaeota*  
778 in Soil. Appl. Environ Microb 78, 6866-6874, DOI: 10.1128/AEM.01681-12,  
779 2012b.

780 Sun, W., Zhang, E., Shulmeister, J., Bird, M.I., Chang, J., Shen, J.: Abrupt changes in  
781 Indian summer monsoon strength during the last deglaciation and early Holocene  
782 based on stable isotope evidence from Lake Chenghai, southwest China.  
783 Quaternary. Sci. Rev. 218, 1-9, DOI: 10.1016/j.quascirev.2019.06.006, 2019.

784 Tian, L., Wang, M., Zhang, X., Yang, X., Zong, Y., Jia, G., Zheng, Z., Man, M.:  
785 Synchronous change of temperature and moisture over the past 50 ka in  
786 subtropical southwest China as indicated by biomarker records in a crater lake.  
787 Quaternary. Sci. Rev. 212, 121-134, DOI: 10.1016/j.quascirev.2019.04.003,  
788 2019.

789 Tierney, J.E., Russell, J.M., Huang, Y., Damst é J.S.S., Hopmans, E.C., Cohen, A.S.:  
790 Northern Hemisphere controls on tropical southeast African climate during the  
791 past 60,000 years. Science 322, 252-255, DOI: 10.1126/science.1160485, 2008.

792 Tierney, J.E., Russell, J.M., Eggermont, H., Hopmans, E.C., Verschuren, D., Damste,  
793 J.S.S.: Environmental controls on branched tetraether lipid distributions in  
794 tropical East African lake sediments. Geochim. Cosmochim. Ac. 74, 4902-4918,  
795 DOI: 10.1016/j.gca.2010.06.002, 2010.

796 Wan, G.J., Chen, J.A., Wu, F.C., Xu, S.Q., Bai, Z.G., Wan, E.Y., Wang, C.S., Huang,  
797 R.G., Yeager, K.M., Santschi, P.H.: Coupling between <sup>210</sup>Pb<sub>ex</sub> and organic matter  
798 in sediments of a nutrient-enriched lake: An example from Lake Chenghai, China.  
799 Chem Geol 224, 223-236, DOI: 10.1016/j.chemgeo.2005.07.025, 2005.

800 Wang, H., Dong, H., Zhang, C.L., Jiang, H., Liu, Z., Zhao, M., Liu, W.: Deglacial and  
801 Holocene archaeal lipid-inferred paleohydrology and paleotemperature history of  
802 Lake Qinghai, northeastern Qinghai–Tibetan Plateau. Quaternary. Res. 83,  
803 116-126, DOI: 10.1016/j.yqres.2014.10.003, 2015.

804 Wang, H., Dong, H., Zhang, C.L., Jiang, H., Zhao, M., Liu, Z., Lai, Z., Liu, W.: Water  
805 depth affecting thaumarchaeol production in Lake Qinghai, northeastern  
806 Qinghai–Tibetan plateau: Implications for paleo lake levels and paleoclimate.

807 Chem. Geol. 368, 76-84, DOI: 10.1016/j.chemgeo.2014.01.009, 2014a.

808 Wang, H., He, Y., Liu, W., Zhou, A., Kolpakova, M., Krivonogov, S., Liu, Z.: Lake  
809 Water Depth Controlling Archaeal Tetraether Distributions in Midlatitude Asia:  
810 Implications for Paleo Lake-Level Reconstruction. *Geophys. Res. Lett.* 46,  
811 5274-5283, DOI: 10.1029/2019GL082157, 2019.

812 Wang, H., Leng, Q., Liu, W., Yang, H.: A rapid lake-shallowing event terminated  
813 preservation of the Miocene *Clarkia* Fossil Konservat-Lagerstätte (Idaho, USA).  
814 *Geology* 45, 239-242, DOI: 10.1130/G38434.1, 2017a.

815 Wang, M., Tian, Q., Li, X., Liang, J., He, Y., Hou, J.: TEX<sub>86</sub> as a potential proxy of  
816 lake water pH in the Tibetan Plateau. *Palaeogeogr. Palaeocl.* 538, 109381, DOI:  
817 10.1016/j.palaeo.2019.109381, 2020.

818 Wang, M., Zheng, Z., Man, M., Hu, J., Gao, Q.: Branched GDGT-based  
819 paleotemperature reconstruction of the last 30,000 years in humid monsoon  
820 region of Southeast China. *Chem. Geol.* 463, 94-102, DOI:  
821 10.1016/j.chemgeo.2017.05.014, 2017b.

822 Wang, Q., Yang, X., Anderson, N.J., Zhang, E., Li, Y.: Diatom response to climate  
823 forcing of a deep, alpine lake (Lugu Hu, Yunnan, SW China) during the Last  
824 Glacial Maximum and its implications for understanding regional monsoon  
825 variability. *Quaternary. Sci. Rev.* 86, 1-12, DOI: 10.1016/j.quascirev.2013.12.024,  
826 2014b.

827 Wang, S., Dou, H.: *Lakes in China*. Science Press, Beijing, China (in Chinese), 1998.

828 Weijers, J.W.H., Schouten, S., Spaargaren, O.C., Damste, J.S.S.: Occurrence and  
829 distribution of tetraether membrane lipids in soils: Implications for the use of the  
830 TEX<sub>86</sub> proxy and the BIT index. *Org. Geochem.* 37, 1680-1693, DOI:  
831 10.1016/j.orggeochem.2006.07.018, 2006.

832 Wu, D., Chen, X., Lv, F., Brenner, M., Curtis, J., Zhou, A., Chen, J., Abbott, M., Yu, J.,  
833 Chen, F.: Decoupled early Holocene summer temperature and monsoon  
834 precipitation in southwest China. *Quaternary. Sci. Rev.* 193, 54-67, DOI:  
835 10.1016/j.quascirev.2018.05.038, 2018.

836 Wu, D., Zhou, A., Chen, X., Yu, J., Zhang, J., Sun, H.: Hydrological and ecosystem

837 response to abrupt changes in the Indian monsoon during the last glacial, as  
838 recorded by sediments from Xingyun Lake, Yunnan, China. *Palaeogeogr.*  
839 *Palaeocl.* 421, 15-23, DOI: 10.1016/j.palaeo.2015.01.005, 2015.

840 Wu, J., Gagan, M.K., Jiang, X., Xia, W., Wang, S.: Sedimentary geochemical  
841 evidence for recent eutrophication of Lake Chenghai, Yunnan, China. *J.*  
842 *Paleolimnol.* 32, 85-94, 2004.

843 Yao, Y., Zhao, J., Bauersachs, T., Huang, Y.: Effect of water depth on the TEX<sub>86</sub> proxy  
844 in volcanic lakes of northeastern China. *Org. Geochem.* 129, 88-98, DOI:  
845 10.1016/j.orggeochem.2019.01.014, 2019.

846 Yang, H., Xiao, W., Słowakiewicz, M., Ding, W., Ayari, A., Dang, X., Pei, H.:  
847 Depth-dependent variation of archaeal ether lipids along soil and peat profiles  
848 from southern China: Implications for the use of isoprenoidal GDGTs as  
849 environmental tracers. *Org. Geochem.* 128, 42-56, DOI:  
850 <https://doi.org/10.1016/j.orggeochem.2018.12.009>, 2019.

851 Zhang, E., Chang, J., Cao, Y., Sun, W., Shulmeister, J., Tang, H., Langdon, P.G., Yang,  
852 X., Shen, J.: Holocene high-resolution quantitative summer temperature  
853 reconstruction based on subfossil chironomids from the southeast margin of the  
854 Qinghai-Tibetan Plateau. *Quaternary. Sci. Rev.* 165, 1-12, DOI:  
855 10.1016/j.quascirev.2017.04.008, 2017a.

856 Zhang, E., Chang, J., Shulmeister, J., Langdon, P., Sun, W., Cao, Y., Yang, X., Shen, J.:  
857 Summer temperature fluctuations in Southwestern China during the end of the  
858 LGM and the last deglaciation. *Earth. Planet. Sc. Lett.* 509, 78-87, DOI:  
859 10.1016/j.espl.2018.12.024, 2019.

860 Zhang, E., Sun, W., Chang, J., Ning, D., Shulmeister, J.: Variations of the Indian  
861 summer monsoon over the last 30 000 years inferred from a pyrogenic carbon  
862 record from south-west China. *J. Quaternary. Sci.* 33, 131-138, DOI:  
863 10.1002/jqs.3008, 2018.

864 [Zhang, E., Wang, Y., Sun, W., Shen, J.: Holocene Asian monsoon evolution revealed](#)  
865 [by a pollen record from an alpine lake on the southeastern margin of the](#)  
866 [Qinghai-Tibetan Plateau, China. \*Clim. Past\* 12, 415-427, DOI:](#)

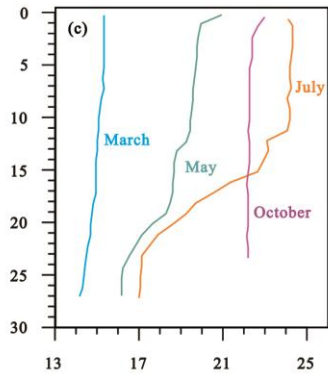
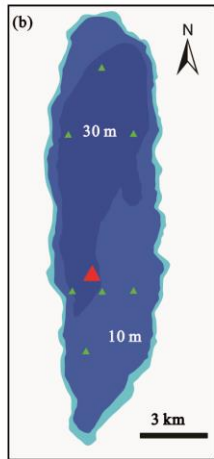
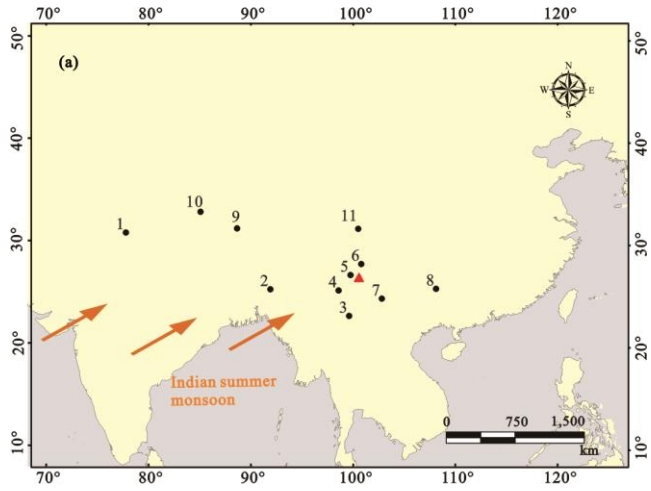
867 | [10.5194/cp-12-415-2016, 2016.](https://doi.org/10.5194/cp-12-415-2016)  
868 Zhang, E., Zhao, C., Xue, B., Liu, Z., Yu, Z., Chen, R., Shen, J.: Millennial-scale  
869 hydroclimate variations in southwest China linked to tropical Indian Ocean since  
870 the Last Glacial Maximum. *Geology* 45, 435-438, DOI: 10.1130/G38309.1,  
871 2017b.  
872 Zheng, Y., Pancost, R.D., Naafs, B.D.A., Li, Q., Liu, Z., Yang, H.: Transition from a  
873 warm and dry to a cold and wet climate in NE China across the Holocene. *Earth*.  
874 *Planet. Sc. Lett.* 493, 36-46, DOI: 10.1016/j.epsl.2018.04.019, 2018.

875

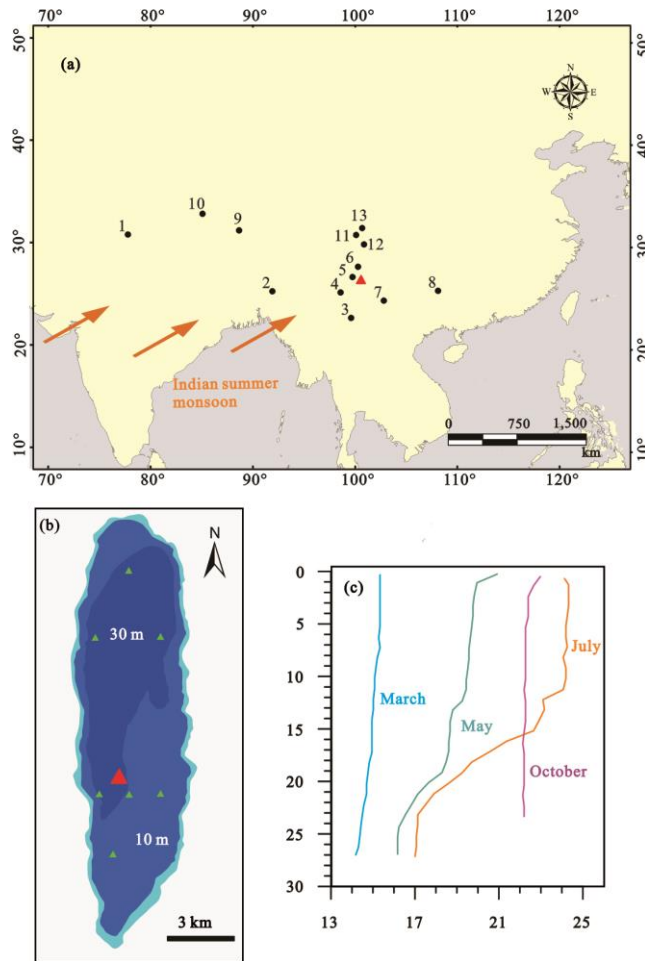
876 **Figure captions**

877





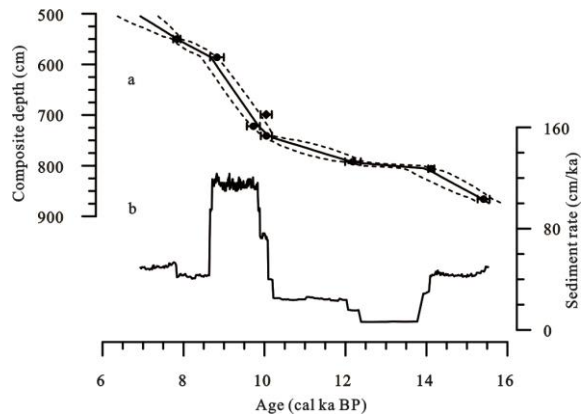
878



879

880 **Fig. 1.** (a) Map showing the location of Lake Chenghai in southwest China (red  
 881 triangle) and other sites (circles) mentioned in the text: 1. Bittoo Cave (Kathayat et al.,  
 882 2016); 2. Mawmluh Cave (Dutt et al., 2015); 3. Lake Ximenglongtan (Ning et al.,  
 883 2019); 4. Lake Tengchongqinghai (Zhang et al., 2017b; Li et al., 2018; Tian et al.,  
 884 2019); 5. Lake Tiancai (Zhang et al., 2017a, 2019); 6. Lake Lugu (Wang et al., 2014);  
 885 7. Lake Xingyun (Wu et al., 2015, 2018); 8. Dongge Cave (Dykoski et al., 2005); 9.  
 886 Nam Co (Günther et al., 2015); 10. Dangxiong Co (Ling et al., 2017); 11. Lake Yidun  
 887 (Shen et al., 2006); 12. Lake Wuxu (Zhang et al., 2016); 13. Lake Muge (Ni et al.,  
 888 2019). (b) The red triangle indicates the location of core CH2016 in Lake Chenghai,  
 889 while green triangles indicate the locations of surface samples. (c) The vertical  
 890 variation of Lake Chenghai water temperature in March, May, July and October (Lu,

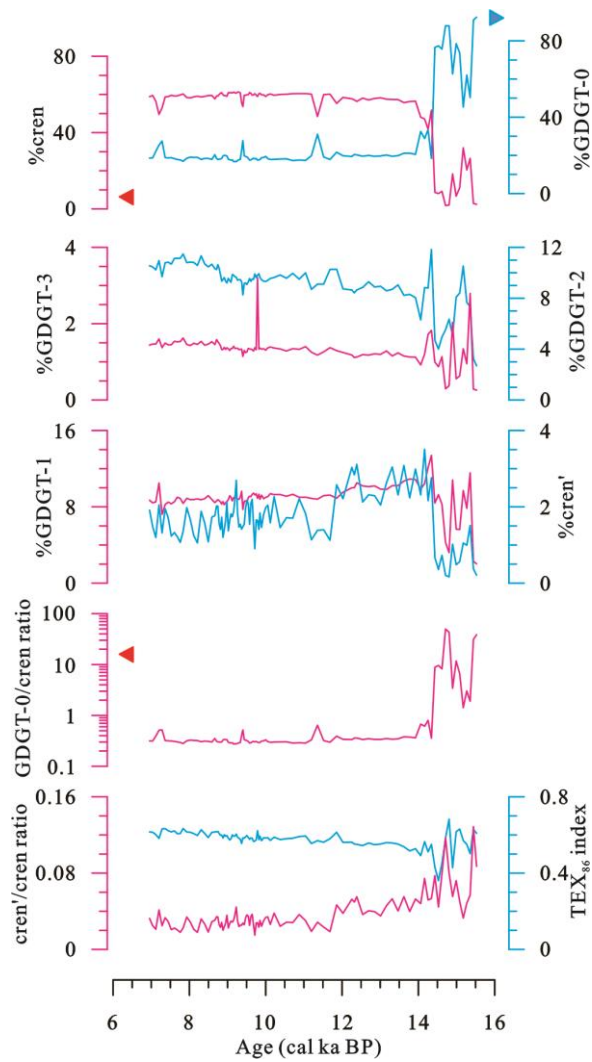
891 2018).

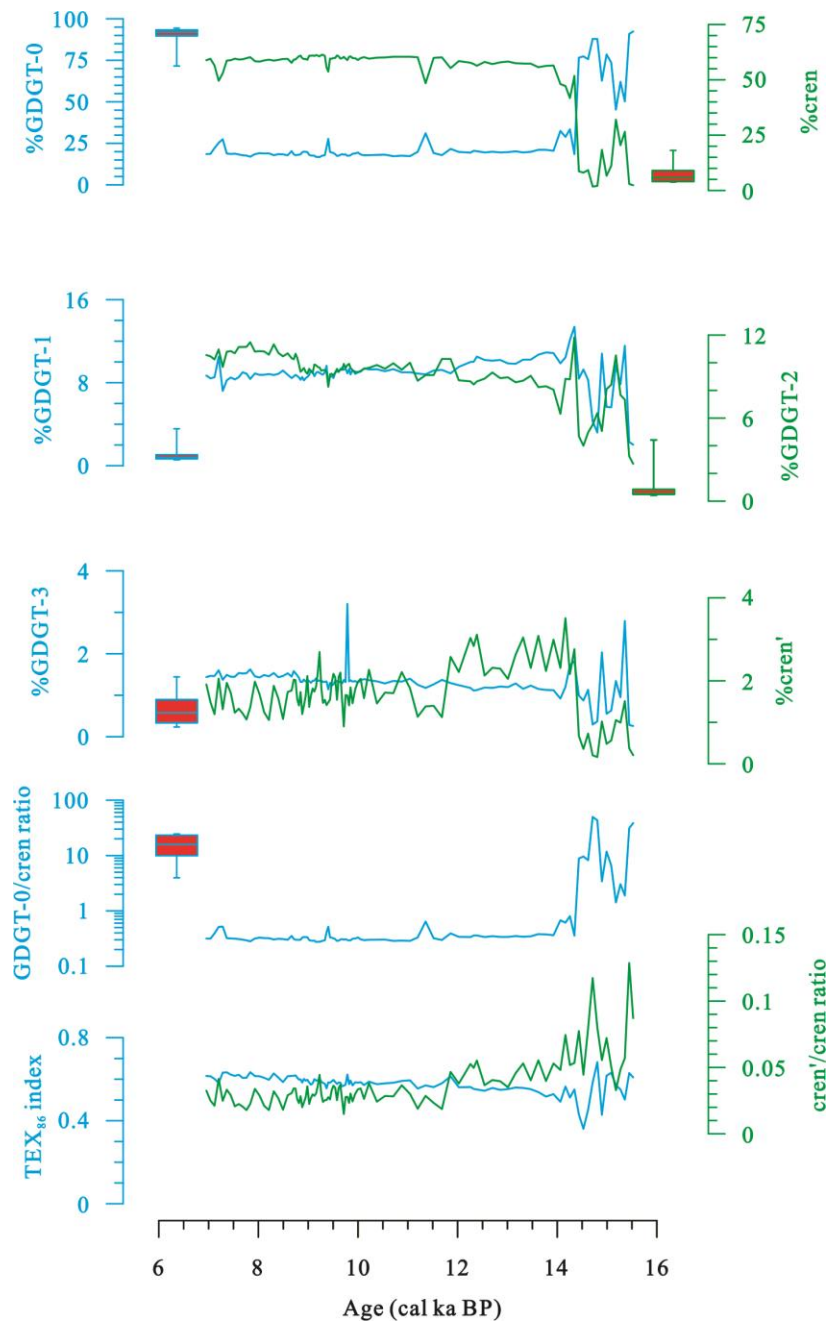


892

893 **Fig. 2.** (a) Age-depth model for the Lake Chenghai sediment core produced using  
894 Bacon software (Blaauw and Andres Christen, 2011) from Sun et al. (2019). Dotted  
895 lines indicate the 95% confidence range and the solid line indicates the weighted  
896 mean ages for each depth, error bars indicate the standard deviation range ( $2\sigma$ ) of the  
897 calibrated radiocarbon dates. (b) estimated sedimentation rate (Sun et al., 2019).

898



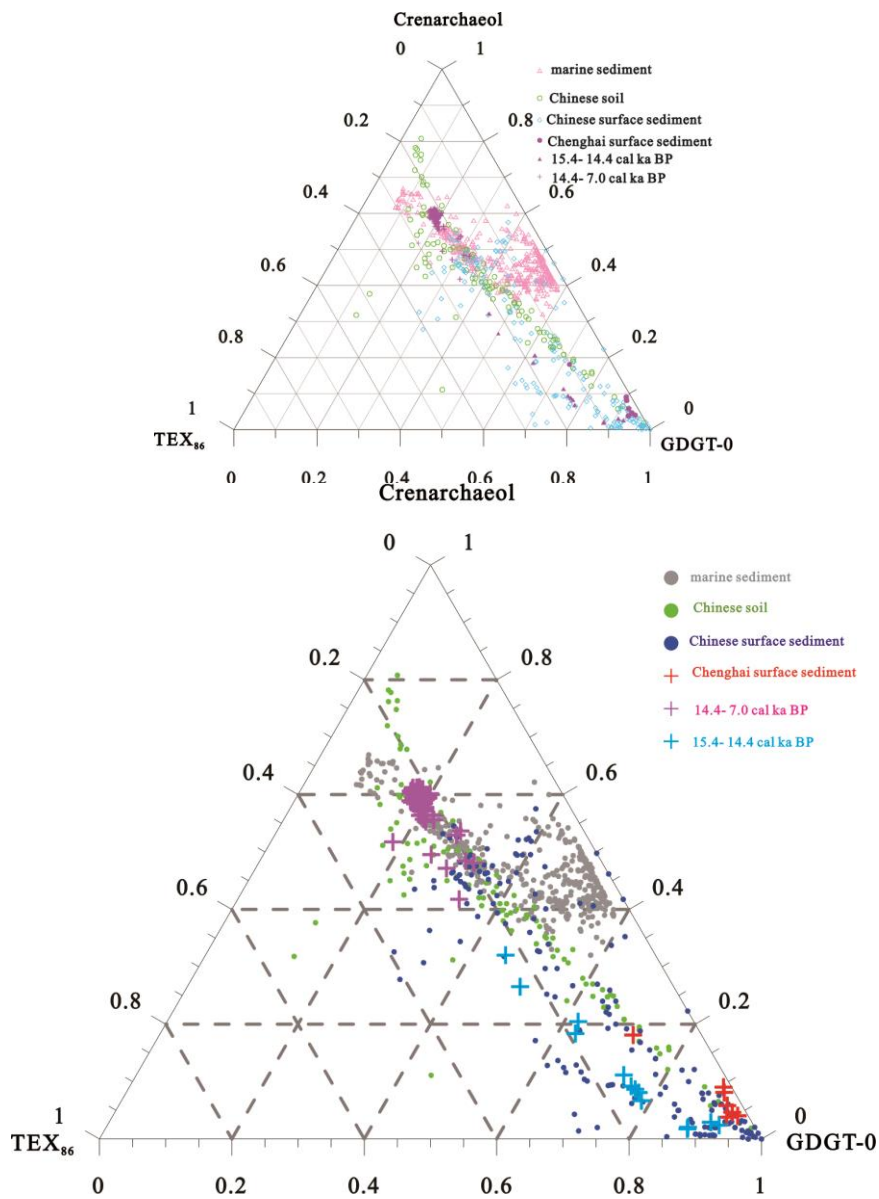


900

901 **Fig. 3.** Variations in the relative isoGDGT distribution and isoGDGTs-based proxies  
 902 of the Lake Chenghai sediment core. The ~~triangles~~ Box-Whisker plots indicate the  
 903 mean values of from surface sediments.

904

905

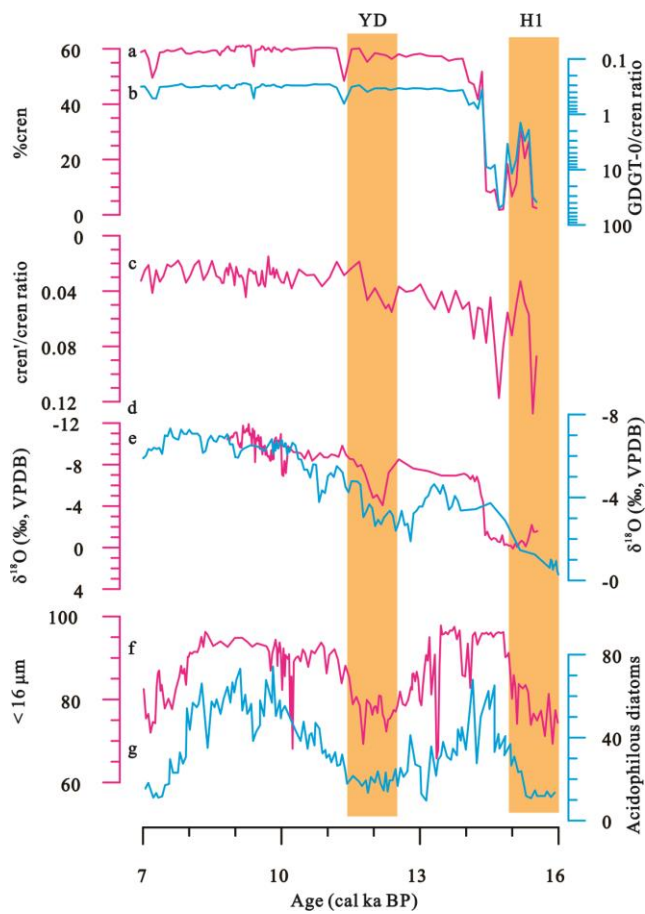


906

907 **Fig. 4.** Ternary diagram showing the distributions of GDGT-0, crenarchaeol, and  
908 'TEX<sub>86</sub>' GDGTs in surface and core sediments from Lake Chenghai, global marine  
909 sediments (Kim et al., 2010), published Chinese soils compiled by Yao et al. (2019),  
910 and Chinese lacustrine surface sediments (G ünther et al., 2014; Dang et al., 2016; Hu  
911 et al., 2016; Li et al., 2016, 2019; Yao et al., 2019; Wang et al., 2020).

912

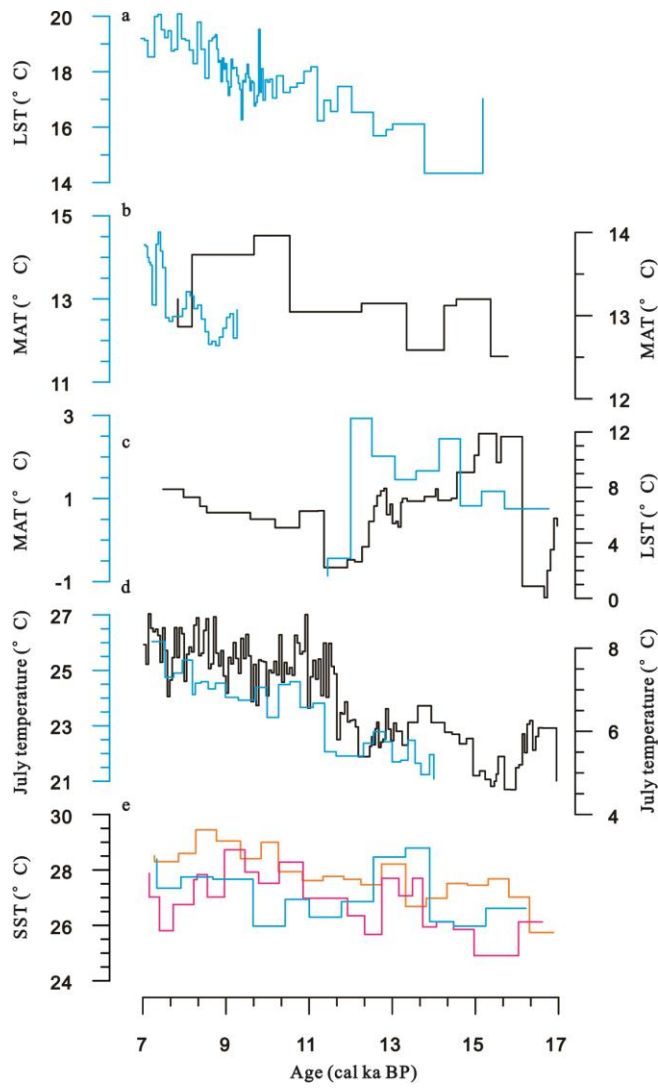
带格式的: 字体: 加粗



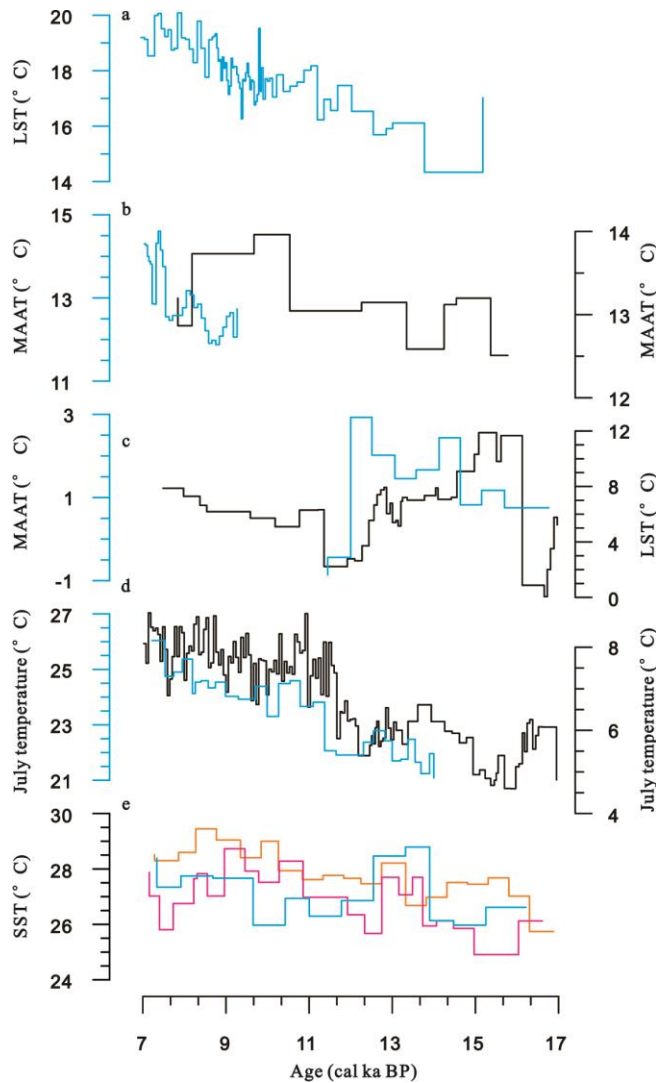
913

914 **Fig. 5.** Comparison of the isoGDGT-based lake-level record from Lake Chenghai (a-c)  
 915 with the  $\delta^{18}\text{O}$  record of carbonate finer in grain size than  $63\ \mu\text{m}$  from Lake Chenghai  
 916 (d, Sun et al., 2019), the stalagmite  $\delta^{18}\text{O}$  records from Mawmluh Cave in northeast  
 917 Indian (e, Dutt et al., 2015); grain-size and diatom record from Lake  
 918 Tengchongqinghai (f and g, Zhang et al., 2017; Li et al., 2018). The shading is utilised  
 919 to represent 'cold' events in the North Atlantic.

920







922

923 **Fig. 6.** A comparison of TEX<sub>86</sub>-based lake surface temperature of Lake Chenghai (a)  
 924 with other paleotemperature records from the ISM region. (b) mean annual  
 925 temperature based on branched GDGTs from Lake Ximenglongtan (blue line, Ning et  
 926 al., 2019) and Lake Tengchongqinghai (black line, Tian et al., 2019); (c)  
 927 Alkenone-based mean annual temperature at Lake Dangxiong (blue line, Ling et al.,  
 928 2017), and TEX<sub>86</sub>-based lake surface temperature of Nam Co from the southern  
 929 Tibetan Plateau (black line, Günther et al., 2015); (d) July temperature reconstructed  
 930 from pollen record from Lake Xingyun (blue line, Wu et al., 2018) and subfossil  
 931 chironomids from Lake Tiancai (black line, Zhang et al., 2017a, 2019);; and (e) sea

932 surface temperatures in the Andaman Sea and Bay of Bengal (Rashid et al., 2007;  
933 Govil and Naidu, 2011; Gebregiorgis et al., 2016).  
934